Development of Radiation Hard N^+-on-P Silicon Microstrip Sensors for Super LHC

Kazuhiko Hara, Koki Inoue, Ai Mochizuki, Tatsuma Meguro, Hiromitsu Hatano, Yoichi Ikegami, Takashi Kohriki, Susumu Terada, Yoshinobu Unno, Kazuhisa Yamamura, and Shintaro Kamata

***Abstract*—Radiation tolerance up to 10^{15} 1-MeV n_{eq}/cm^2 is required for the silicon microstrip sensors to be operated at the Super LHC experiment. As a candidate for such sensors, we are investigating non-inverting n^+-on-p sensors. We manufactured sample sensors of 1 × 1 cm in 4″ and 6″ processes with implementing different interstrip electrical isolation structures. Industrial high resistive p-type wafers from FZ and MCZ growth are tested. They are different in crystal orientations $\langle 100 \rangle$ and $\langle 111 \rangle$ with different wafer resistivities. The sensors were irradiated with 70-MeV protons and characterized in views of the leakage current increase, noise figures, electrical strip isolation, full depletion voltage evolution, and charge collection efficiency.**

***Index Terms*—Microstrip detector, p-bulk silicon, radiation assurance.**

I. Introduction

THE LHC machine, currently at the final tuning stage, is expected to provide proton-proton collisions at luminosity of 10^{34} cm^{-2} s^{-1}. In the ATLAS detector, Semiconductor Tracker (SCT) employs silicon microstrip sensors in the region between 30 cm and 51 cm from the beam pipe [1], [2]. The sensors are p^+-on-n, which are radiation tolerant up to 2×10^{14} 1-MeV n_{eq}/cm^2, corresponding to the fluence for 10 years of LHC operation. Extended operation is limited since the full depletion voltage V_{FD} will exceed 350 V, which is quite close to the voltage rating 500 V of the system.

Super LHC, where the luminosity will reach 10^{35} cm^{-2} s^{-1}, is regarded as the next step to improve the statistical situation for physics reaches beyond the mid 2010's. The inner most part of the tracking will be covered by pixel devices, as for the present ATLAS, then followed by short-strip (2.4 cm) silicon sensors to manage the increased particle density. At the anticipated location of the short-strip sensors ($r = 25$ cm), the estimated fluence ranges from 5.2 to 8.0×10^{14} n_{eq}/cm^2, depending on the distance from the interaction point from $z = 0$ to 3 m, for an integrated luminosity of 3000 fb^{-1} without taking any safety factor [3]. Roughly one half is due to protons and other particles directly from the interaction, and the rest is due to neutrons. To cope with the increased radiation environment, the new SCT should be tolerant at least up to $\sim 1 \times 10^{15}$ 1-MeV n_{eq}/cm^2. We started our R&D in 2004 to develop n^+-on-p sensors. Sensors with p-type wafers are selected since the pn junction stays at the strip side even after receiving radiation. This allows the sensors to remain operational even with the bias below V_{FD}. Therefore n^+-on-p sensors should be usable after receiving high radiation where V_{FD} exceeds the voltage rating of the system. Actually the HV cables of the SCT system should be re-used and the 500 V rating should be applied. The collectable charge will be reduced at partial depletion. However, the S/N should be acceptable since the strip length will be shortened (2.4 cm with respect to the present 12 cm) and the electrical noise will be reduced, accordingly. Alternative choice would be an n^+-on-n sensor, which is employed for the present ATLAS Pixel detector. This, however, requires both side processing and is not suitable for microstrip sensors of large quantity. Thinned sensors may also be interesting, which requires intensive R&D.

Silicon microstrip sensors so far have been manufactured utilizing mainly n-type wafers. There is no exception for large scale detectors, although small quantity R&D works exist for p-type wafers [4], [5], [6], [7]. Positive charges inherently trapped in the oxide layer accumulate a layer of mobile electrons in the silicon surface between the readout strips, which may prevent their independent operation. Technologies such as p-stop and p-spray [8], [9] have been successfully adopted for double-sided p^+-n-n^+ strip sensors and n^+-on-n sensors. Similar structure is required for n^+-on-p sensors [4]. The availability of high resistive p-type wafers was also an issue for depressing adoption of p-type wafers. Recent years, p-type MCZ (magnetic Czochralski) wafers become available, together with "conventional" p-type FZ (float zone) wafers. The primary goal of our R&D is to fabricate radiation tolerant silicon sensors using industrial p-type wafers available to Hamamatsu Photonics (HPK), one of the companies who have ability of large scale production required.

The sensors reported in this paper were fabricated first with 4″ process and then with 6″ process. The strip isolation structures and doping densities were modified in these productions. The wafer makers are also different. Radiation damage on the

Manuscript received June 14, 2008; revised January 17, 2009. Current version published April 08, 2009

K. Hara, T. Meguro, and H. Hatano are with the Institute of Pure and Applied Sciences, University of Tsukuba, Tsukuba, Ibaraki 305-8571, Japan (e-mail: hara@px.tsukuba.ac.jp; meguro@hep.px.tsukuba.ac.jp; hatano@hep.px.tsukuba.ac.jp).

K. Inoue was with the University of Tsukuba, Tsukuba, Ibaraki 305-8571, Japan. He is now with NEC Ltd., Tokyo, Japan (e-mail: inoue@hep.px.tsukuba.ac.jp).

A. Mochizuki was with the University of Tsukuba, Tsukuba, Ibaraki 305-8571, Japan. She is now with Toshiba Company, Minato-ku, Tokyo 105-8001, Japan (e-mail: mocizuki@hep.px.tsukuba.ac.jp).

Y. Ikegami, T. Kohriki, S. Terada, and Y. Unno are with the Institute of Particle and Nuclear Studies, High Energy Accelerator Research Organization, KEK, Tsukuba, Ibaraki 305-0801, Japan (e-mail: yoichi.ikegami@kek.jp; takashi.kohriki@kek.jp; susumu.terada@kek.jp; unno@post.kek.jp).

K. Yamamura and S. Kamata are with the Solid State Division, Hamamatsu Photonics, Hamamatsu, Shizuoka 435-8558, Japan (e-mail: yamamura@ssd.hpk.co.jp; skamata@ssd.hpk.co.jp).

Color versions of one or more of the figures in this paper are available online at http://ieeexplore.ieee.org.

Digital Object Identifier 10.1109/TNS.2009.2014162

0018-9499/$25.00 © 2009 IEEE

TABLE I
LIST OF THE SAMPLES. THE PREFIX 4 OR 6 REFERS TO THE WAFER SIZE (INCHES), FZ IS FLOAT ZONE, MC IS MAGNETIC CZOCHRALSKI. LISTED ARE RESISTIVITY, CRYSTAL ORIENTATION, P-STOP AND P-SPRAY CONCENTRATIONS

Sample	ρ (kΩcm)	Orient'n	p-stop (/cm²)	p-spray (/cm²)
4FzP	6	<111>	2×10^{12}	2×10^{12}
4FzL	6	<111>	5×10^{12}	
4FzH	6	<111>	20×10^{12}	
4McP	0.8	<100>	2×10^{12}	2×10^{12}
4McL	0.8	<100>	5×10^{12}	
4McH	0.8	<100>	20×10^{12}	
6FzP	5	<100>	8×10^{12}	2×10^{12}
6FzM	5	<100>	10×10^{12}	
6FzH	5	<100>	20×10^{12}	
6FzpP	5	<100>	8×10^{12}	2×10^{12}
6FzpM	5	<100>	10×10^{12}	
6FzpH	5	<100>	20×10^{12}	
6McP	2	<100>	8×10^{12}	2×10^{12}
6McM	2	<100>	10×10^{12}	
6McH	2	<100>	20×10^{12}	

bulk is dependent on the material property, hence on the wafer growth techniques primarily and sensor fabrication as well. The strip isolation needs to be optimized to achieve sufficient electrical isolation also after irradiation while not introducing defective leakage current increase. The optimization should depend on the surface property, which is dependent on the wafer quality including the crystal orientation and also on the sensor fabrication technique. The fabricated test sensors were irradiated with 70-MeV protons up to 5×10^{15} 1-MeV $\mathrm{n_{eq}/cm^2}$. The sensor performance was evaluated before and after irradiation through dark current leakage vs. bias (IV), bulk capacitance vs. bias (CV), interstrip resistance (Isolation), and charge collection (CC) efficiency measurements. The details of the samples and irradiation procedure are described in Section II. The pre- and post irradiation characterization procedures and results are given in Section III. Section IV describes the summary.

II. SAMPLES AND PROTON IRRADIATION

A. Samples

Table I summarizes the characteristics of the evaluated samples. The outer dimensions are 10 mm × 10 mm and 0.3 mm thickness, the strip length being 8 mm. The strip structure is identical to the present SCT, 16 μm wide implant strips spaced at an 80 μm pitch with each strip connected to the common bias ring via 1.5-MΩ poly-silicon resistor. The 22 μm wide Al electrodes are AC coupled, extending over the implant strips.

Two p-stop concentrations ("H", and "L" or "M") and one p-spray concentration (2×10^{12} /cm²) were tried each for 4″ and 6″ samples, as summarized in Table I. The p-spray was subjected to the samples (with "P" in Sample name) with a low p-stop concentration such that the sum concentration at the p-stop channels is equivalent to the p-stop only samples with lower concentration (with "L" for 4″ and "M" for 6″). As the lower concentration for 4″ turned out to be too small, we increased the concentration ("M") for 6″. Note that the concentration values should be regarded as indicative only. For 6″ we employed two types of FZ wafers, Fz and Fzp. Fzp wafers contain fewer defects than standard Fz.

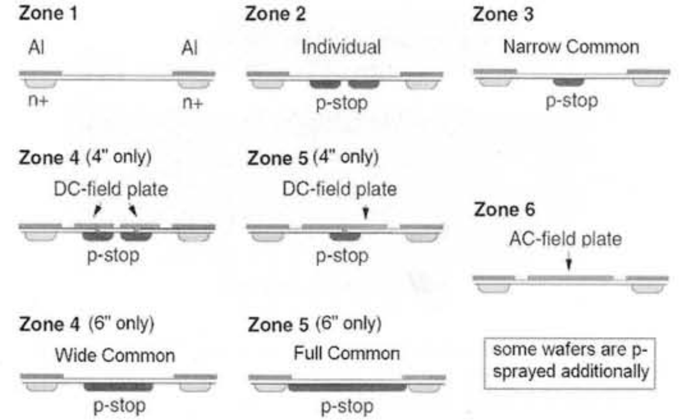

Fig. 1. Electrical strip isolation structures, Z1 to Z6, implemented for 4″ and 6″ processes. The field plates for Z4 to Z6 are poly-silicon. The structures with DC field plates Z4 and Z5 in 4″ are modified to wider and full wide p-stop in 6″. Three p-stop concentrations were examined with p-spray added to the lowest concentration.

On a wafer basis, we have implemented six different strip isolation structures including one with no structure. The structures are illustrated in Fig. 1 [10]. Zone 1 (Z1) has no structure; Z2 and Z3 have individual and common p-stop structures, respectively; Z6 has no p-stop but with poly-silicon electrodes on top of oxide insulators (AC field plates). The poly-silicon potential can be controlled externally to eliminate the electron accumulation underneath utilizing the MOS effect. Z4 and Z5 are differently implemented for 4″ and 6″ processes. In 4″, they are similar to Z2 and Z3 but with poly-silicon electrodes DC connected to the p-stop implants. Since the effects of DC plates turned out to be not significant, we modified them in 6″ to wider (Z4) or fully wide (Z5) common p-stop electrodes.

B. Proton Irradiation

The proton irradiation was performed with 70-MeV protons at CYRIC, Tohoku University. The facility and early irradiation results are described elsewhere [11]. The NIEL [12] conversion factor 1.4 is adopted to take into account the damage ratio of 70-MeV protons to 1-MeV neutrons. For 4″ samples, six fluence points $(1, 2, 5, 10, 20, 50) \times 10^{14}\ \mathrm{n_{eq}/cm^2}$ were chosen, while $50 \times 10^{14}\ \mathrm{n_{eq}/cm^2}$ was omitted for 6″.

Three (for 4″) or six (for 6″) samples were glued and wire-bonded per printed-circuit board (PCB) for electrical characterization, see Fig. 2. About 10 such PCBs were stacked along the beam, and exposed to protons to the planned fluence. During the irradiation, the samples were cooled at $-10^\circ\mathrm{C}$ and kept biased at 100 V. In order to achieve uniform exposure for the finite beam size (5-15 mm FWHM), the samples were scanned in the beam continuously. The irradiation periods were several minutes to hours depending on the fluence. The energy loss along the beam was evaluated with GEANT4, which is not significant in view of NIEL factors.

The actual proton fluence was evaluated through the reaction $^{27}\mathrm{Al(p,x)}^{24}\mathrm{Na}$ and detecting 1.368 MeV γ's from $^{24}\mathrm{Na}$ decay with a calibrated Ge detector. The uncertainty of the fluence

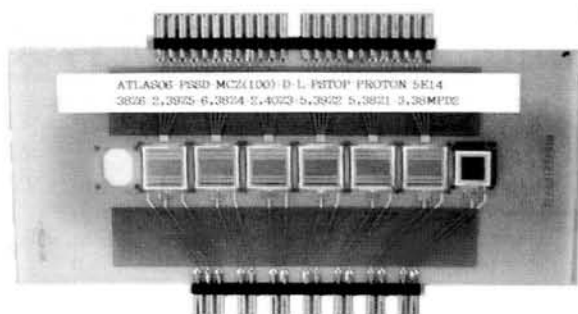

Fig. 2. Printed circuit board for 6″ irradiation, containing Z1 to Z6 test samples (with a test diode at right) and traces for biasing and signal readout. The beam profile is visible as darker area around the samples.

is dominated by that of the reaction cross-section, which is no more than 10%. The achieved uniformity was checked using Fujifilm imaging plates [13] that detect γ-rays generated in Al foil.

III. Performance Characterization and Results

A. Characterization Procedure

The irradiated samples were undertaken the annealing process at 60°C for 80 min to settle the initial recovery. Except during this annealing process and characterization measurements, the samples were stored in at -20°C.[1]

The electrical properties IV, CV, and strip isolation were measured for every sample by placing the test PCB board in a light-tight thermostat chamber. The temperature was set at 20°C before and -20°C after the irradiation. In these measurements the bias was raised up to 1 kV at a step of 10 V. With the CV, the capacitance between the bias-ring and the backplane was measured with an LCR meter at a test frequency of 1 kHz. The strip isolation was evaluated by the current when 5 V was applied across a pair of implant electrodes at neighbor. If the interstrip resistance is large enough, the current should read 1.7 μA determined by the two bias resistors and two implant resistances in series.

Since the current of the irradiated samples increases substantially and may deteriorate the noise performance, we measured the noise using an SCT ABCD3T readout chip and DAQ system [16], [17]. In order to simulate the performance of 2.4-cm long strip detector, a candidate for super LHC, three strips at neighbor were wire-bonded in series to other two remote sets of three strips. Thus, three neighboring 2.4-cm long strips were made and wire-bonded to the specific channels of the ABCD3T chip. In changing the sample, the same channels were used to eliminate the gain difference in the ABCD3T channels. The measurement was made for 4″ samples with high p-stop concentration since the noise originating in the isolation structure may be most significant.

[1]The applied annealing is a recommended procedure to minimize the variation due to different irradiation conditions such as accelerated irradiation time (see, for example, Ref. [14]). The characteristics of irradiated sensors further changes with time unless the samples are kept at low temperature. Storing at -20°C can suppress such changes, and hence can control the history of irradiated silicon sensors. The annealing property of the tested wafers is reported in [15].

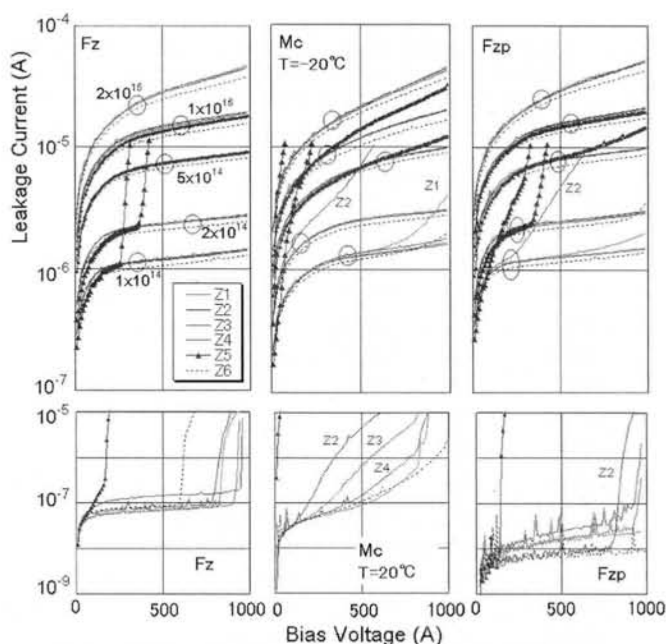

Fig. 3. IV curves for 6″ samples with p-spray (6FzP, 6McP and 6FzpP). The upper curves are after irradiation measured at -20°C for 5 fluence values, and lower curves are before irradiation measured at 20°C. No Z5 data for 2×10^{15} $/\mathrm{cm}^2$ for sample availability.

The charge collection was measured as a function of bias by injecting a collimated infrared laser light [18] between the specified strips and measuring the amplified signals of the two strips with a digital oscilloscope. The amplifiers are of current amplifiers. The peaking time is 20 ns for the laser signal, similar to the SCT electronics. The temperature was typically -10°C on the sample PCB, controlled by a cooled block underneath and cooled N_2 gas. The gas flushing was effective to prevent thermal runaway. On the same block, a reference Si sensor was located. We repeatedly measured the reference to monitor and normalize the laser power. We chose Z6 sensors for this study.

B. Leakage Current, IV

Examples of IV curves are plotted in Fig. 3 for 6″ samples with p-spray. For the pre-irradiation data, which are available for each fluence value, only typical sets are plotted. The pre-irradiation leakage current is about one order lower for Fzp than the others, as explained by fewer defects. The typical current 10 nA/cm2 for Fzp, however, is a level similar to "standard" n-type sensors, implying that "standard" p-type wafers available to HPK are of lower quality compared to n-type wafers. Note that many small spikes seen in the pre-irradiation curves are equipment problems; the averaging time of the ampere-meter is too short to measure such small leakage current. The micro-discharge, a steep leakage current increase above some bias, is often seen in pre-irradiation data. The plotted FZ data, except for Z5, show micro-discharge onset voltages exceeding 500 V, which seem better than MCZ data. Any conclusion, however, requires accumulation of more data to statistically understand the difference.

Most of the micro-discharges disappear after irradiation except for Z5 (with triangles in plots), for which the electric field at

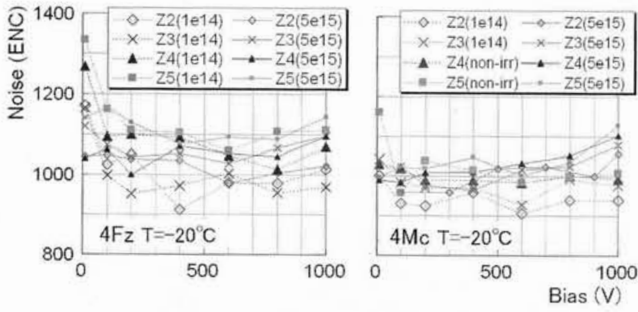

Fig. 4. The noise values for 4FzH and 4McH samples, shown for two sets of radiation fluences, 1×10^{14} (FZ) or non-irradiation (MCZ), and 5×10^{15} /cm^2.

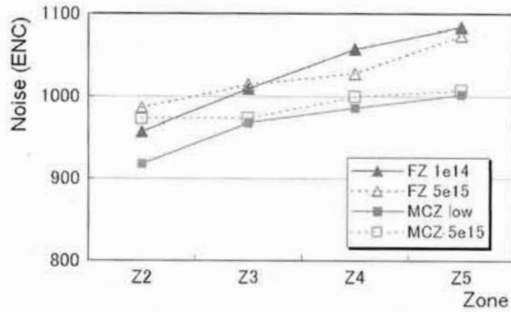

Fig. 5. The noise values averaged for the bias range from 300 to 700 V, shown for 4FzH and 4McH samples. MCZ low is 10^{14} /cm^2 or non-irradiated.

the n^+/p-stop boundary should be too large. The leakage current after irradiation resembles among the samples, while Z6 (in broken curves in plots) shows systematically smaller current. There is small difference also for other samples with high and middle p-stop concentrations. The damage constant ranged from 3.3 to 4.0×10^{-17} A/cm^3, which is consistent with the value known [14] for n-type wafers.

C. Noise

The noise results are shown in Fig. 4 for 4″ samples 4FzH and 4McH. The samples were cooled to $-20°$C. The noise of un-connected channels of this ABCD3T chip distributed in the range 700-850 ENC. The noise figures of the three connected channels increased and were almost similar among them with the central channel showing a noise slightly larger than the neighbors (50 ENC at maximum). The noise decreases with the bias as the strip isolation is established (see Section III-D). This tendency is more distinct for FZ, or the isolation of MCZ samples is established from low bias voltages.

Fig. 5 shows the zone dependence at two fluence values, highest fluence 5×10^{15} /cm^2 and the lowest fluence or non-irradiation (for sample availability). The samples Z4 and Z5 with DC filed plates showed larger noise than Z2 and Z3. There is no clear dependence on the fluence, i.e., on the increased leakage current. Comparing to the nominal noise 1500 ENC of the present SCT detector with 124 mm long strips, the irradiated short-strip detector exhibits smaller noise as expected.

D. Strip Isolation

The strip isolation is achieved as the bias voltage is increased, as shown in Fig. 6 where the data for 6FzH samples irradiated to 2×10^{15} /cm^2 are shown as examples. We define the isolation

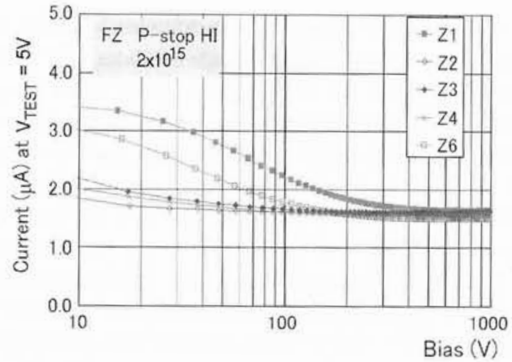

Fig. 6. Strip isolation for 6″ Fz with high p-stop concentration, irradiated to 2×10^{15} /cm^2. The AC field of Z6 is floating.

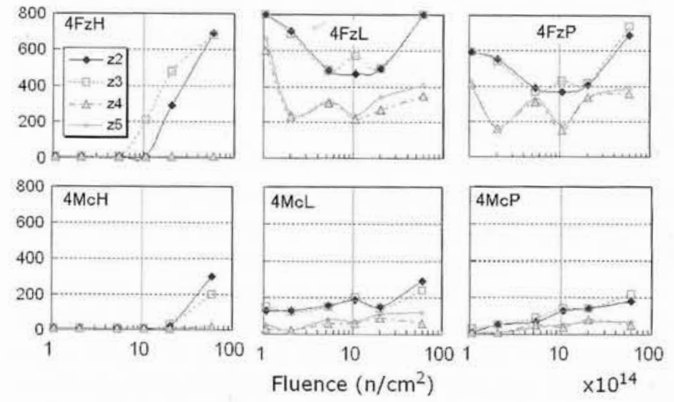

Fig. 7. Strip isolation voltages [V] of 4″ Fz (upper) and MCZ (lower) samples for three p-stop concentrations (H, L, P in Table I). Z1 samples were not irradiated and Z6 data are not plotted.

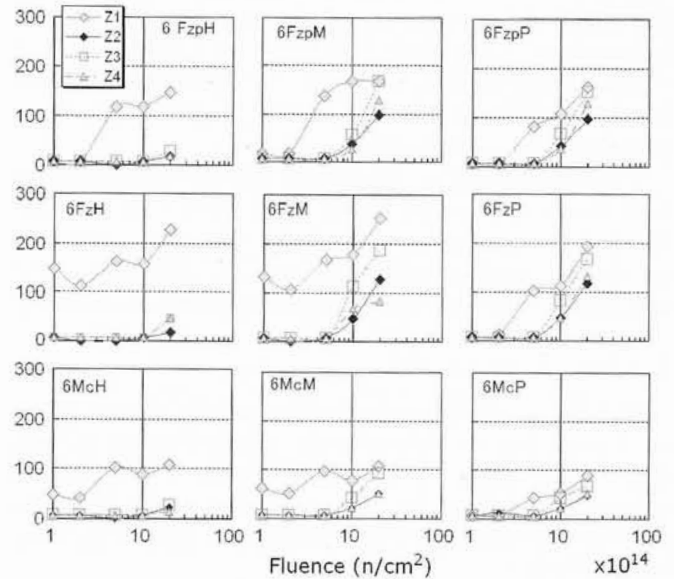

Fig. 8. Strip isolation voltages [V] of 6″ Fzp (upper), Fz (middle) and MCZ (lower) for three p-stop concentrations (H, M, P in Table I). Z5 and Z6 data are not plotted. Z1 has no structure (H and M), or has p-spray only (P).

voltage as the bias where the current reaches the value 10% larger than the asymptotic current at high bias.

In Figs. 7 and 8, the isolation voltages are plotted as a function of the fluence for 4″ and 6″ samples, respectively. From the 4″

data, we conclude that p-stop concentration of 5×10^{12} /cm^2 is too small, because an isolation voltage of about 800 V (200 V) is required for Z2 and Z3 of FZ (MCZ), even at the lowest fluence while it is nearly zero for the samples with high p-stop concentration. For the samples with p-spray, sum concentration 4×10^{12} /cm^2 at the p-stop channel is also too weak. These samples (L and P) show a tendency that the isolation voltage decreases with fluence up to 1×10^{15} /cm^2, and then turns to increase. The pre-irradiation isolation voltages are different among the samples, depending on the sample location in the wafer, for example. This is the reason for the substructure deviating from the above general tendency. Some effectiveness of DC field plates (Z4 and Z5) is seen only for these samples with low p-stop concentrations.

The isolation of 4″ MCZ samples is better than 4″ FZ. This is most probably due to the difference in the crystal orientations since the improvement from 4″ FZ $\langle 111 \rangle$ to 6″ FZ $\langle 100 \rangle$ is substantial while there is little difference between 4″ MCZ and 6″ MCZ, both being $\langle 100 \rangle$.

From the data for 6″ samples, the isolation voltages of middle concentration samples (M and P) increased more than of high concentration samples (H) at fluence above 1×10^{15} /cm^2. However, the required bias, 150 V at maximum for FZ, is still small compared to the full depletion voltages and is manageable. Concerning the different wafer growths, MCZ seems better in general than FZ. We note that the isolation of Fzp Z1 where no isolation structure is present is established from zero bias. The necessity of the strip isolation structure for n^+-on-p sensors should be entirely dependent on the Si irregularity probability at the surface. The isolation of Fzp Z1, however, starts to degrade above 5×10^{14} /cm^2 and implementing some isolation such as p-spray is preferred. In fact, p-spray only process is considered as a promising candidate since the performance of other wafers becomes as good as Fzp and the pre-irradiation individual difference should be reduced. It also requires fewer masks and hence fewer process steps.

The isolation with AC field plates (Z6) functioned successfully. The sample suitable for this study is 4″ FZ since the isolation of Z1 is not complete. Typically -60 V was required to establish the isolation with the back bias at -200 V. For MCZ and irradiated samples, the required voltages were even lower.

E. Charge Collection, CC

The charge collection was evaluated for Z6 samples where the pulsed laser was spotted at the defined location between the strips. Fig. 9 shows typical oscilloscope traces for irradiated samples. The pulse height does not change more than 5% for 5 μm deviations about the nominal position, positioning being better than 5 μm.

The peak voltages are plotted in Figs. 10 and 11 for 4″ and 6″ samples, measured every 25 V. The peak voltage can be translated to the input charge with the amplifier gain 3 mV/fC. We use these curves to extract the full depletion voltages and to evaluate CC of irradiated samples, normalized by the pre-irradiation data.

The full depletion voltages are defined as the intercepts of two straight lines in C^2-V plots. The straight line can be obtained unambiguously in the region below V_{FD}. For the evaluation in the plateau region, the CC is averaged in the middle

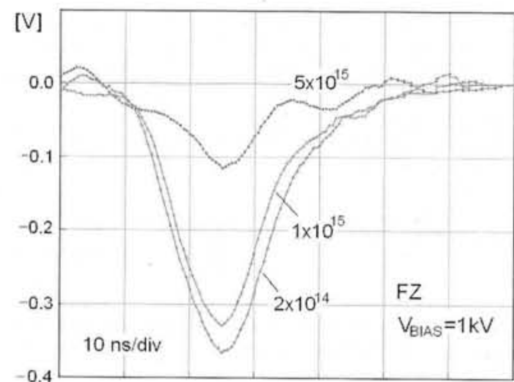

Fig. 9. Oscilloscope traces of 4″ FZ samples at 1 kV bias irradiated to $(2, 10, 50) \times 10^{14}$ /cm^2. The magnitude of peak voltage decreases with the fluence.

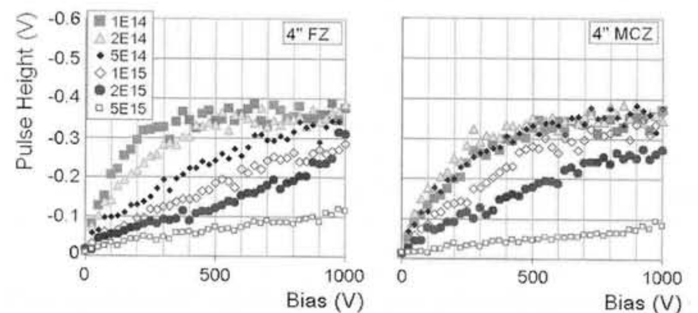

Fig. 10. Charge collection curves for 4Fz (left) and 4Mc (right) samples, for fluence values from 1 to 50×10^{14} /cm^2.

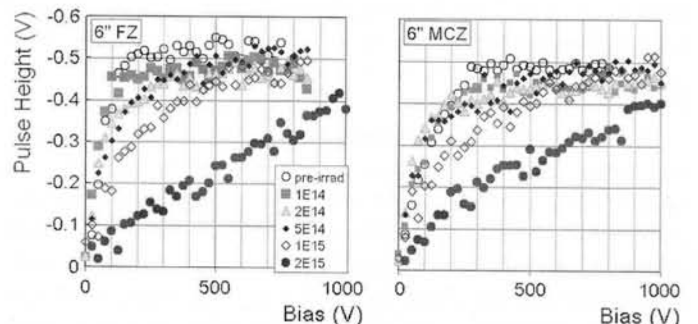

Fig. 11. Charge collection curves for 6Fz (left) and 6Mc (right) samples, compared between before and after irradiation for fluence values from 1 to 20×10^{14} /cm^2.

$(400 < V_B < 600$ V) and high $(600 < V_B < 800$ V) bias regions, and the difference is assigned as the systematic uncertainty. The results are shown in Fig. 12 for 4″ and 6″ data. Although the initial V_{FD}'s are different, the fluence dependences are similar among 4″ MCZ and 6″ samples, showing a decrease up to fluence of a few $\times 10^{14}$ /cm^2, above which V_{FD} increases gradually. The only exception is 4″ FZ, showing a much steeper increase. Natural interpretation of this difference is the wafer orientation. Oxygen richness is one of the parameters to determine the radiation hardness [14]. A SIMS analysis was carried out to measure the oxygen concentrations, resulting $(7.5 \pm 0.3, 5.3 \pm 0.2, 2.6 \pm 0.2$ and $4.6 \pm 0.3) \times 10^{17}$ atoms/cm^3 at the

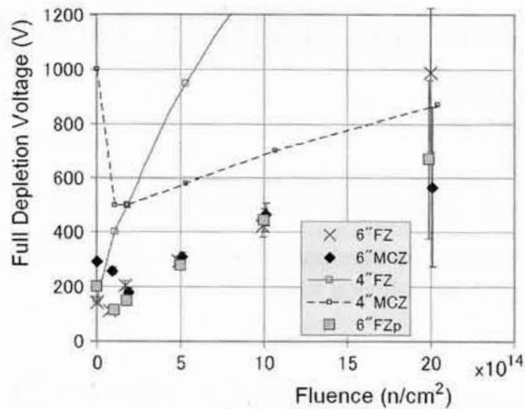

Fig. 12. Full depletion voltages for three 6″ wafers as a function of fluence. The data for 4″ wafers, shown in curves, have uncertainties similar to 6″ data.

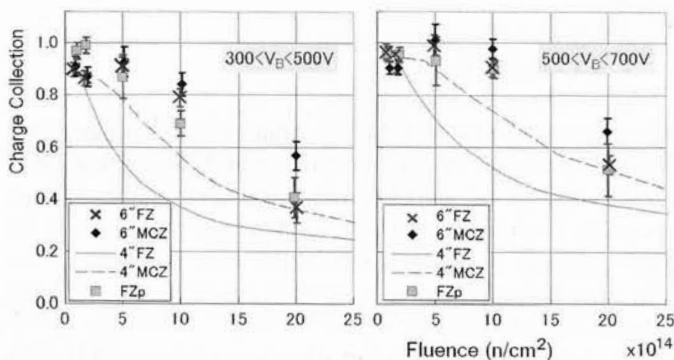

Fig. 13. Charge collection averaged in two bias regions, as a function of fluence for three 6″ wafers. The data for 4″ wafers, shown in curves, have uncertainties similar to 6″ data. Additional overall uncertainty is 10%.

middle of the wafers for (4Fz, 4MCZ, 6Fz and 6MCZ), respectively.[2] The radiation hardness difference among these wafers can not be explained by the oxygen richness alone. In fact, the wafer manufacturers of 4Fz and 6Fz are different, as well as the wafer orientation: $\langle 111 \rangle$ for 4Fz, and $\langle 100 \rangle$ for others.

Since n^+-on-p sensors have an advantage that they are operational with biases below V_{FD}, evaluation of CCs under such biases is of prime importance. As mentioned before, 500 V is the critical voltage in this evaluation. In Fig. 13, we plot the CCs averaged in two bias regions, $300 < V_B < 500$ V and $500 < V_B < 700$ V, as a function of fluence. The average CCs for 6″ are similar in the two regions since the sensors are almost at fully depletion. They are approximately 50% at 2×10^{15} /cm^2. For 4″ wafers, CCs are smaller since they are definitely under partial depletion. Since the charge collections of 4″ samples at 1 kV bias, for example, are similar to those of 6″ samples, there is little difference among the wafers in the maximum collectable amount of charges.

IV. Summary

We have fabricated n^+-on-p microstrip sensors using industrial FZ and MCZ wafers. They were irradiated with protons up to 5×10^{15} 1-MeV n_{eq}/cm^2 and tested for electrical properties and charge collection.

The strip isolation is better with $\langle 100 \rangle$ wafers. They require a bias of 200 V at most to achieve isolation even without p-stop or p-spray. Adding uniform p-spray may enhance the reliability especially in the low fluence range up to 5×10^{14} /cm^2. Above this fluence, the isolation starts to degrade. The degradation is minimum for the samples with p-stop of high concentration.

Among the tested wafers, 4″ and 6″ MCZ, and 6″ FZ showed similar full depletion voltage evolution with fluence, reaching approximately 500 V at 1×10^{15} /cm^2. Wafers of 4″ FZ exhibited significantly degraded performance. The drop of charge collection can be maintained to 50% for 6″ wafers at 500 V after 2×10^{15} /cm^2.

The tested 6″ wafers are good candidates for microstrip sensors for Super LHC experiment.

[2]The primary ions, Cs at 5 keV, were injected to the sample shared at the middle perpendicular to the shared cross section. The measured oxygen concentration decreased initially reaching a constant beyond 1 μm depth. The quoted values are the average and rms of the data in the depth range between 2.5 to 5.0 μm. The overall normalization uncertainty is 5%.

Acknowledgment

We express our acknowledgment to T. Shinozuka and T. Wakui of CYRIC for their continuous supports, and to the CYRIC operation crews for performing excellent irradiation.

References

[1] A. Abdesselam *et al.*, "The barrel modules of the ATLAS semiconductor tracker," *Nucl. Instrum. Methods Phys. Res. A*, vol. A568, pp. 642–671, 2006.

[2] A. Abhmad *et al.*, "The silicon microstrip sensors for the ATLAS semiconductor tracker," *Nucl. Instrum. Methods Phys. Res. A*, vol. A578, pp. 98–118, 2007.

[3] I. Dawson, "Radiation simulations and irradiation facilities," in *Proc. ATLAS Tracker Upgrade Workshop*, Liverpool, U.K., Dec 6–8, 2006.

[4] S. Terada *et al.*, "Proton irradiation on p-bulk silicon strip detectors using 12 GeV PS at KEK," *Nucl. Instrum. Methods Phys. Res. A*, vol. A383, pp. 159–165, 1996.

[5] M. Bruzzi *et al.*, "Radiation-hard semiconductor detectors for SuperLHC," *Nucl. Instrum. Methods Phys. Res. A*, vol. A541, pp. 189–201, 2005.

[6] G. Casse *et al.*, "First results pn charge collection efficiency of heavily irradiated microstrip sensors fabricated on oxygenated p-type silicon," *Nucl. Instrum. Methods Phys. Res. A*, vol. A518, pp. 340–342, 2004.

[7] G. Pellegrini *et al.*, "Technology development of p-type microstrip detectors with radiation hard p-spray isolation," *Nucl. Instrum. Methods Phys. Res. A*, vol. A566, pp. 360–365, 2006.

[8] G. Batignani *et al.*, "Development of double side readout silicon strip detectors," *Nucl. Instrum. Methods Phys. Res. A*, vol. A273, pp. 677–681, 1988.

[9] R. H. Richter *et al.*, "Strip detector design for ATLAS and HERA-B using two-dimensional device simulation," *Nucl. Instrum. Methods Phys. Res. A*, vol. A377, pp. 412–421, 1996.

[10] Y. Unno, "Silicon sensors for development for the ATLAS upgrade for SLHC," *Nucl. Instrum. Methods Phys. Res. A*, vol. A569, pp. 41–47, 2006.

[11] Y. Unno *et al.*, "p-bulk silicon microstrip sensors and irradiation," *Nucl. Instrum. Methods Phys. Res. A*, vol. A273, pp. 677–681, 2007.

[12] A. Vasilescu and G. Lindström, Note on the Fluence Normalization Based on the NIEL Scaling Hypothesis, ROSE/TN/2002-02, 2000.

[13] Fujifilm Bio-Imaging Analyzer (BAS Series) FUJIFILM Co. [Online]. Available: http://fujifilm.jp/business/lifescience/simaging/bas/index.html

[14] G. Lindström *et al.*, "Radiation hard silicon detectors—Developments by the RD48 (ROSE) collaboration," *Nucl. Instrum. Methods Phys. Res. A*, vol. A466, p. 308, 2001.

[15] K. Hara *et al.*, "Characteristics of the irradiated Hamamatsu p-bulk silicon microstrip sensors," in *Proc. IEEE Nuclear Science Symp.*, Dresden, Germany, Oct. 19–25, 2008.

[16] F. Campabadal *et al.*, "Design and performance of the ABCD3TA ASIC for readout of silicon strip detectors in the ATLAS semiconductor tracker," *Nucl. Instrum. Methods Phys. Res. A*, vol. A552, pp. 292–328, 2005.

[17] Y. Unno *et al.*, "Application of Cu-polyimide flex circuit and Al-on-glass pitch adapter for the ATLAS SCT barrel hybrid," *Nucl. Instrum. Methods Phys. Res. A*, vol. A541, pp. 286–294, 2005.

[18] K. Hara *et al.*, "Test of ATLAS SCT barrel modules with Nd:YAG laser," *Nucl. Instrum. Methods Phys. Res. A*, vol. A541, pp. 122–129, 2005.